Articles

Kinetics and Oxygen Vacancy Mechanism of the Oxidation of Carbon Monoxide on Perovskite $Nd_{1-x}Sr_xCoO_{3-y}$ Solutions as a Catalyst

Dong Hoon Lee and Keu Hong Kim*

Department of Chemistry, Yonsei University, Seoul 120-749, Korea
Received March 5, 1994

The oxidation of carbon monoxide by gaseous oxygen in the presence of a powdered $Nd_{1-x}Sr_xCoO_{3-y}$ solid solution as a catalyst has been investigated in the temperature range from 150°C to 300°C under various CO and O_2 partial pressures. The site of Sr substitution, nonstoichiometry, structure, and microstructure were studied by means of powder X-ray diffraction and infrared spectroscopy. The electrical conductivity of the solid solution has been measured at 300°C under various CO and O_2 partial pressures. The oxidation rates have been correlated with 1.5- and 1.2-order kinetics with and without a CO_2 trap, respectively; first- and 0.7 order with respect to CO and 0.5- order to O_2. For the above reaction temperature range, the activation energy is in the range from 0.25 to 0.35 eV/mol. From the infrared spectroscopic, conductivity and kinetic data, CO appears essentially to be adsorbed on the lattice oxygens of the catalyst, while O_2 adsorbs as ions on the oxygen vacancies formed by Sr substitution. The oxygen vacancy mechanism of the CO oxidation and the main defect of $Nd_{1-x}Sr_xCoO_{3-y}$ solid solution are supported and suggested from the agreement between IR data, conductivities, and kinetic data.

Introduction

The catalytic oxidation of carbon monoxide has been studied at a test reaction to investigate the variation of catalytic activity of $NdCoO_3$ by Sr substitution. It is well known that the catalytic activities of metallic oxides are correlated with their nonstoichiometric composition and electronic properties. In this point of view, the Sr was incorporated to change the nonstoichiometry of $NdCoO_3$. On the other hand, a correlation between the catalytic activity and the *d*-electron configuration in metallic oxide has been found to exist in the catalytic of carbon monoxide. It has been reported that the catalytic activity of metallic increases with increase in the empty *d*-orbital of metal ion[1] and the backbonding between π^*-orbital of CO and *d*-orbital of metal ion is a key to determine the catalytic activities of perovskite oxides on the CO oxidation[2].

Kiss and Gonzalez[3] observed that the rates of CO oxidation on SiO_2 supported Rh catalyst decrease with increasing the oxidation state of Rh catalyst. For the present catalysts, it is expected from the Sr substitution that variation of the oxidation state of Co in the $Nd_{1-x}Sr_xCoO_{3-y}$ acts as an important role for the enhancement of the catalytic activity. We accordingly prepared the $Nd_{1-x}Sr_xCoO_{3-y}$ catalysts doped with different atomic mol fraction of Sr and characterized them by X-ray diffraction analysis and infrared spectroscopy.

Experimental

Material Preparation

The $Nd_{1-x}Sr_xCoO_{3-y}$ powder. Appropriate weights of the Nd_2O_3 (99.99%), $SrCO_3$ (99.999%), and CoO (from Co_3O_4, 99.995%) powders obtained from the Aldrich Co. were mixed in ethanol and stirred for 72h to obtain a homogeneous dispersion. The mixture was then filtered and dried at 150°C. This mixed and dried powder was put on a covered platinum crucible, placed in a preheated furnace, and fired in air at 1050°C for 72h and then slowly cooled to room temperature. The fired powder was ball-milled for 2h, calcined at 900°C, and then cooled rapidly to room temperature. Some of the mixed powders was fired in air at 1000 and 900°C for 72h and then slowly cooled to room temperature.

The $Nd_{1-x}Sr_xCoO_{3-y}$ pellet. Some of the powder prepared by the above procedure was compressed under a pressure of 19.6 MPa into a pellet and sintered at 400°C for 2h. After sintering, the sample was given a light abrasive polish onto faces until the voids were fully eliminated, and then cut into a rectangular shape with suitable dimensions in order to measure the electrical conductivity.

Reactant gases. CO was prepared from the reaction of $CaCO_3$ and Zn powder in mole ratio of 1 : 2. The chemical reaction was carried out by heating them at about 700°C in quartz tube connected to CO gas storage. O_2 was obtained from Matheson Gas Products (99.98% purity) and used after purification. The CO and O_2 were purified by passing them over glass wool, $CaCl_2$ and P_2O_5. This purification was found to give CO and O_2 sufficiently free of catalytic poisons for the catalytic reactions.

Nonstoichiometry and Surface Area

x and y values. The x value in $Nd_{1-x}Sr_xCoO_{3-y}$ catalyst was confirmed by atomic absorption spectroscopy (AAS). The effective values of x are 0.247, 0.493, and 0.739 in accordance with the nominal values of 0.250, 0.500 and 0.750, respectively. Based on the AAS data, the effective values of x are almost the same as the nominal values, satisfying within the experimental errors. The y value was calculated by determining the amounts of Co^{4+} and the total amount of Co. The

Kinetics, Mechanism, CO Oxidation, $Nd_{1-x}Sr_xCoO_{3-y}$

Bull. Korean Chem. Soc. **1994**, Vol. 15, No. 8   617

total amount of Co was determined following the procedure reported by Gushee *et al.*[4]. The amounts of Co^{4+} and Co^{3+} were also determined according to the reported procedure[5]. The values of y are 0.001 ($x=0$), 0.008 ($x=0.25$), 0.059 ($x=0.50$), and 0.103 ($x=0.75$), respectively.

Surface area. The surface area of each sample (100-160 mesh) was measured by a Blain test. The measured surface area increases with increasing x value, indicating 2.01 ($x=0$), 3.87 ($x=0.25$), 4.93 ($x=0.50$), and 5.05 m^2/g ($x=0.75$), respectively.

Structure Analysis

X-ray analysis. Powder X-ray diffraction was performed on a diffractometer (Philips, model PW 1710, $CuK\alpha$) equipped with a curved graphite monochromator in a selected beam path. The crystal structure of each sample was deduced from the diffraction pattern. Based on the power X-ray diffraction data, the accurate lattice parameter (a) for each sample was determined in the same manner as described in the previous papers[6-11]. The lattice parameter (7.548 Å) of pure $NdCoO_{2.999}$ agrees with the ASTM listing ($a=7.546$ Å). The a-values for various Sr-substituted samples were obtained from the same method. The a-values obtained for the $Nd_{1-x}Sr_xCoO_{3-y}$ catalysts are plotted against atomic mol fraction of Sr.

Infrared spectra. The infrared spectra of crystals extracted from KBr pellets were recorded at room temperature using a Shimadzu IR-435 spectrometer[12]. The infrared spectra of pure CoO and Co_3O_4 crystals were also recorded in order to obtain informations for microcrystal structure and site of Sr substitution in the $Nd_{1-x}Sr_xCoO_{3-y}$ crystals.

Measurement of the Electrical Conductivity and Reaction Rate

Conductivity. The electrical conductivity measurements were performed in the temperature range of 150-300℃ under various CO and O_2 partial pressures. The conductivity measurement circuitry and the four-probe model were previously described[13,14]. The details of the experimental apparatus, instruments, and calculations of measured conductivity have been reported in the previous papers, for examples, on catalysts[15-17] polymer composites[18-20], organic polymers[21-23], oxide semiconductors[24-27] and high-Tc superconductors[28,29].

Reaction rate. The high-vacuum system was connected to a reaction chamber (142 m*l*), CO and O_2 gas storage tanks, Baratron pressure guage, electrometers, lock-in amplifier, potentiometers, gas chromatographs (silicagel, molecular sieve, or Porapak Q), electrical furnace, liquid nitrogen trap, and small other instruments. The catalytic oxidation reactions of CO were performed at 150-300℃ with 0.4-0.5 g of catalyst on the reaction chamber bed. The rates of reduction by CO and oxidation by O_2 of the catalyst were measured by the pressure changes, respectively. The product CO_2 was condensed by a liquid nitrogen trap and measured. The amounts of CO and O_2 consumptions were evaluated from the pressure changes and the measured CO_2, respectively. In order to confirm the evaluated values, the product was checked by CO_2 sensor (Thomas 5220).

The conductivities were measured in the reaction temperature range under the partial pressures of CO and O_2. Prior to the conductivity measurement, the pellet-catalysts were always pretreated with CO and O_2 for 30 min at 300℃ and
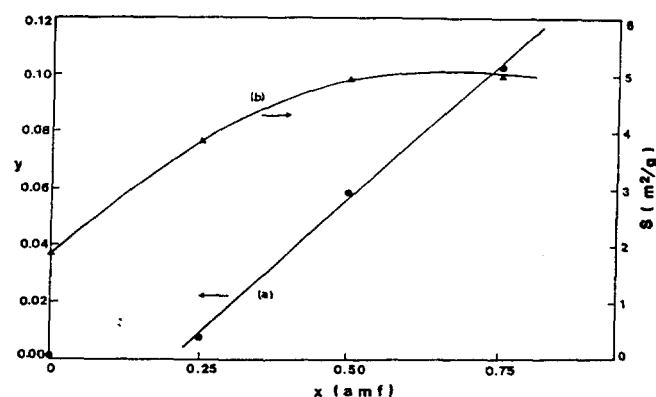

Figure 1. The nonstoichiometry (y) and surface area (S) dependences of the amount (x, atomic mol fraction) of Sr substitution in $Nd_{1-x}Sr_xCoO_{3-y}$ catalysts.

then degassed for 1h at 400℃ and 1×10^{-3} Torr. A gas mixture of CO, O_2 and N_2 was used for flow experiments with the flow rate of 30-50 m*l*·min^{-1}. Sometimes, the balance of the gas mixture ($CO+O_2=30\%$) was maintained by He carrier gas instead of N_2. The product was analyzed by a gas chromatograph.

Results and Discussion

Relationship between Sr Substitution (x) and Non-stoichiometry (Y). The stoichiometric $SrCoO_3$ is obtained by continuous heating at 1000℃ under a total static pressure of 65 kbar after heating a mixture of Sr and Co nitrates in a stream of oxygen at 900℃[30]. This $SrCoO_3$ has a cubic perovskite structure with lattic parameter $a=3.840$ Å.

We had a series experiment to prepare $SrCoO_3$, that is, $x=1$ in $Nd_{1-x}Sr_xCoO_3$; A mixture of $SrCO_3$ and CoO powders was heated at 1100℃ for 24h in air, and then the fragile product was regrinded, pelleted, and reheated at that temperature for 12h in air. The final product was $SrCoO_{2.8}$ with tetragonal structure. The composition was determined by the comparison with the reported JCPDS files. When the above mixture was continuonsly heated at 1100℃ in air for 36h, the product was the mixture of $SrCoO_{2.8}$ which was major and $SrCoO_{2.29}$ with cubic structure. If one of the starting materials and heating temperature were changed to Co_3O_4 and 910℃, a mixture of $SrCoO_{2.8}$ and $SrCoO_{2.5}$ (hexagonal structure) was obtained.

Based on the results of our series experiment, the stoichiometric $SrCoO_3$ may not be prepared by the same preparing procedures and conditions as $Nd_{1-x}Sr_xCoO_3$ where $0 \leq x \leq 0.75$.

Figure 1(a) shows that the nonstoichiometry (y) increases with increasing amount of Sr substitution. At $x=0$, the value 0.001 of y in our quenched sample is very close to the reported value of 0.0011 in vacuum treated sample[31], but is somewhat different from $y=0$ in pretreated sample at 300℃ in oxygen atmosphere[31]. As shown in Figure 1(a), $y=0.001$ at $x=0$ is very deviated from the data on the straight line. Based on the present data in Figure 1(a) and reported values of 0.0011 and zero in the vacuum treated and oxygen atmosphere, respectively, the nonstoichiometry of $Nd_{1-x}Sr_xCoO_{3-y}$ more easily and linearly increases due to Sr substitution
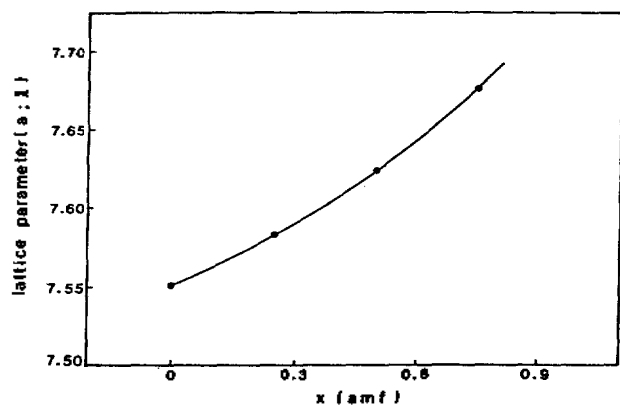
Figure 2. The lattice parameter (a) vs the amount (x) of Sr substitution in $Nd_{1-x}Sr_xCoO_{3-y}$ catalysts.

rather than due to treatment conditions of the sample.

The surface area(s) of the present quenched catalyst increases with increasing Sr substitution up to $x=0.50$ ($S=4.93$ m^2/g), as shown in Figure 1(b), but is nearly constant for further increase in Sr substitution, showing 5.05 m^2/g at $x=$ 0.75, the maximum. The maximum value of 5.4 m^2/g at $x=0.4$ for the O_2-pretreated sample[31] is similar to the present value, while the surface area abruptly decreases from 5.4 $(x=0.4)$ to 3.5 m^2/g $(x=0.6)$. This is very interesting in the variation of surface area between the quenched and O_2-pretreated samples.

Structure and Microstructure. The plot of lattice parameter (a) vs atomic mol fraction (x) of Sr is shown in Figure 2. The a-value (7.548 Å) at $x=0$ obtained by the least squares methods agrees with the value (7.546 Å) listed in ASTM. In Figure 2, the lattice parameter increases with increasing Sr substitution up to $x=0.75$, showing small deviation from the linearity. This result can be explained by the different ionic radii between Nd and Sr ions. Since the ionicradius of Sr ($Sr^{2+}=158$ pm) is larger than that of Nd (Nd^{3+} $=141$ pm), the lattice parameter (a) increases with increasing Sr addition. However, unfortunately, the result is also satisfied by the Sr substitution for Co, since the radius of Sr^{2+} is continuously larger than those of Co ($Co^{3+}=68.5$ pm and $Co^{4+}=67$ pm). Only with the data in Figure 2, it is difficult to confirm the microstructure of $Nd_{1-x}Sr_xCoO_{3-y}$ catalysts.

In order to solve this problem, the infrared spectra were recorded and analyzed. Figure 3(a) and (b) show the infrared spectra of CoO and Co_3O_4, respectively. In Figure 3(a), a single absorption band appears at 560 cm^{-1}, which is assigned to Co-O vibration due to CoO_6, since CoO has NaCl structure. However, in Figure 3(b), four absorption bands are observed, because the Co_3O_4 has spinel structure in which Co^{3+} and Co^{2+} locate in oictahedral and tetrahedral sites, respectively. The two infrared bands at 510 and 580 cm^{-1} are considered to be due to the Co-O vibrations of Co^{2+} and $Co^{3+}O_6$ in the normal spinel structure, respectively. The bands at 530 and 560 cm^{-1} are possibly originated from the inverse spinel structure in which some of the Co^{3+} ions locate in the tetrahedral sites. Based on the four observed infrared bands, the present Co_3O_4 is slightly deviated from the normal spinel structure.

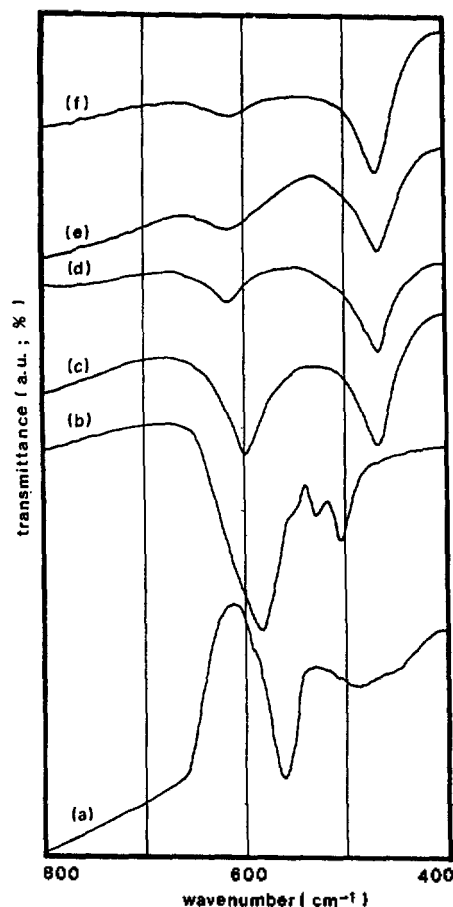Figure 3(c), (d), (e), and (f) show the infrared spectra of

Figure 3. The infrared spectra of pure CoO, Co_3O_4, and Nd_{1-x} Sr_xCoO_{3-y}: (a) CoO, (b) Co_3O_4, (c) $x=0$, (d) $x=0.25$, (e) $x=0.50$, and (f) $x=0.75$ in $Nd_{1-x}Sr_xCoO_{3-y}$ catalysts.

$Nd_{1-x}Sr_xCoO_{3-y}$ for $x=0$ (c), $x=0.25$ (d), $x=0.50$ (e), and $x=$ 0.75 (f), respectively. The $NdCoO_{3-y}$ structure is pseudo-cubic, but its octahedral symmetry of Co is conserved. As can be seen in Figure 3(a) and (b), the vibrational band due to octahedral Co is observed at 570 cm^{-1}. On the other hand, the infrared hand due to same octahedral Co in $NdCoO_{3-y}$ does at 470 cm^{-1}, as shown in Figure 3(c)-(f). This implies that the bond nature of Co-O in CoO and Co_3O_4 is different from that in $NdCoO_{3-y}$. On the order hand, in Figure 3(c)-(f), the intensities and frequencies of the 470 cm^{-1} bands are almost unchanged as the amount of Sr incorporated in $NdCoO_{3-y}$ increases, but those of 600 cm^{-1} bands are changed. This indicates that the band at 600 cm^{-1} is originated from NdO vibration in $NdCoO_{3-y}$, and implies that the Sr incorporated in $NdCoO_{3-y}$ enters into the Nd position and then increases the nonstoichichiometry.

This increase of degree of the nonstoichiometry was confirmed by the infrared spectra. Figure 4 shows the infrared spectra recorded with $NdCoO_{3-y}$ samples which were prepared at different temperatures. The intensity of 600 cm^{-1} band increases with decreases in sintering temperatures in the sequence of 1050 (c), 1000 (b), and 900°C (a). This was also observed on $Nd_{0.5}Sr_{0.5}CoO_{3-y}$ samples. As can be seen in Figure 5, the intensity of 620 cm^{-1} band increases with decreases in the same sintering temperatures as $NdCoO_{3-y}$.
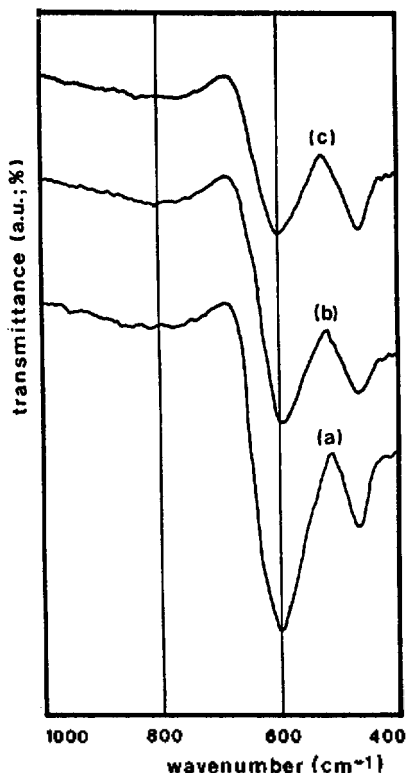
Figure 4. The infrared spectra of pure $NdCoO_{3-y}$ catalysts which were sintered at 900 (a), 1000 (b), and 1050℃ (c) in air, respectively.
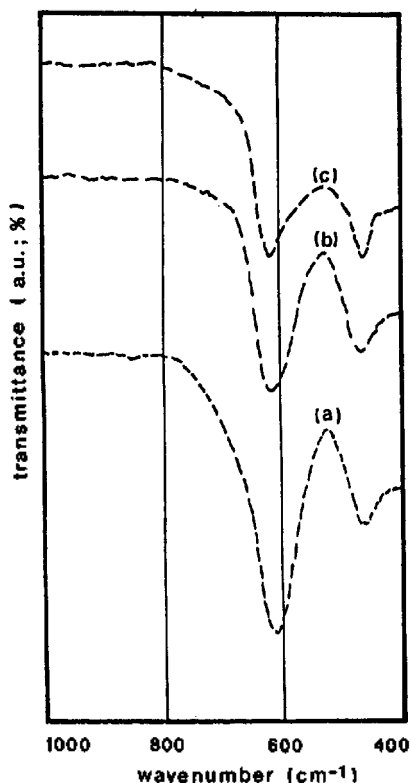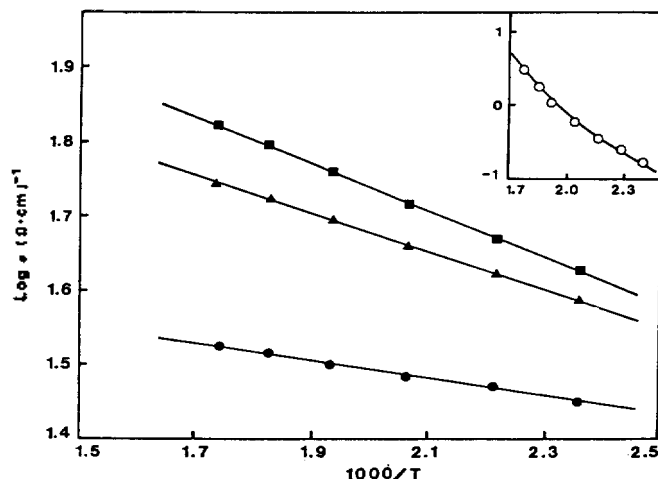

Figure 6. Temperature dependence of electrical conductivity at constant P_{O_2} of 1×10^{-5} atm for $Nd_{1-x}Sr_xCoO_{3-y}$ catalyst sintered at 1050℃. The values of x in $Nd_{1-x}Sr_xCoO_{3-y}$ are 0.00 (○), 0.25 (●), 0.50 (▲) and 0.75 (■).

Table 1. Temperature Dependence of Specific Rate (k, $Torr^{-0.5}\cdot min^{-1}\cdot g^{-1}$) and Activation Energy (Ea, eV) of CO Oxidation on $Nd_{1-x}Sr_xCoO_{3-y}$

T (℃)		150	200	250	300	Ea
x	y					
0.25	0.008	2.14×10^{-6}	6.31×10^{-6}	1.26×10^{-5}	2.24×10^{-5}	0.33
0.50	0.059	5.39×10^{-5}	1.43×10^{-4}	2.15×10^{-4}	3.22×10^{-4}	0.25
0.75	0.103	5.01×10^{-4}	1.32×10^{-3}	3.16×10^{-3}	6.31×10^{-3}	0.35

On the other hand, in Figures 4 and 5, the intensity of 470 cm^{-1} band is almost unchanged, even though the sintering temperature and amount of Sr are varied. These results imply that the degree of nonstoichiometry depends upon the concentration of oxygen atom which is bonded with Nd atom. From the infrared spectra in Figures 3-5, it is concluded that the Sr incorporated in $NdCoO_3$ substitutes for Nd, and as a result, the nonstoichiometry is originated from the oxygen atom bonded with Nd atom.

Electrical Conductivity and Kinetics. The electrical conductivity as shown in Figure 6 increases with increasing temperatures and amounts of Sr from $x=0$ to $x=0.75$ in $Nd_{1-x}Sr_xCoO_{3-y}$. However, the temperature dependence of electrical conductivity for $NdCoO_{3-y}$ catalyst is different from those for $NdCoO_{3-y}$ doped with Sr, showing two different kinds of slope behaviors. The increasing conductivity with increasing amounts of Sr indicates that Sr substitution for Nd produces electrons into donor level by the disorder equilibrium $O^{2-} = \frac{1}{2} O_2(g) + V_o + 2e^-$ where O^{2-} is a lattice oxygen, V_O an oxygen vacancy and e^- an electron.

On the other hand, the electrical conductivity increases with partial pressures of carbon monoxide (P_{CO}), but decreases with partial pressures of oxygen (P_{O_2}). From the conductivity data shown in Table 3 and activation energy in Table 1, it is suggested that the reactants may be adsorbed on the surface of catalyst. At the surface of catalyst, the charge

Figure 5. The infrared spectra of $Nd_{0.5}Sr_{0.5}CoO_{3-y}$ catalysts sintered at 900 (a), 1000 (b), and 1050℃ (c) in air, respectively.

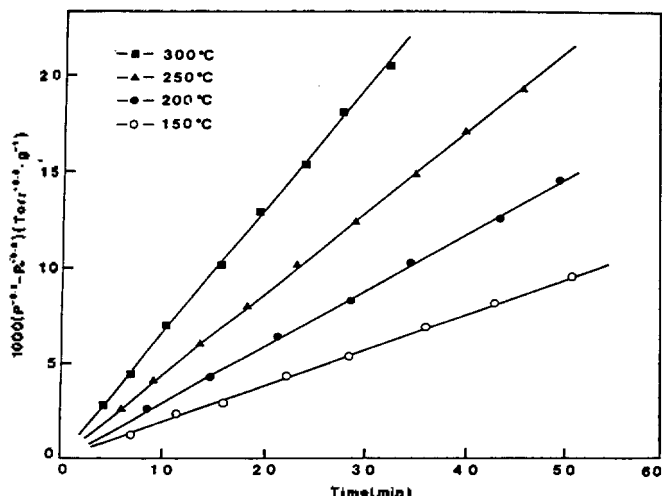620 *Bull. Korean Chem. Soc.* **1994**, Vol. 15, No. 8

Dong Hoon Lee and Keu Hong Kim

Figure 7. Representative oxidation rates of CO on $Nd_{0.5}Sr_{0.5}$-$CoO_{2.94}$ at various temperatures. $P^0_{CO}=120$ Torr; $P^0_{O_2}=60$ Torr; catalyst$=0.4$ g; surface area$=4.93$ m^2/g (100-160 mesh); P^0, total initial pressure; p, total pressure.

transfer forming a double layer may be interpreted in terms of a space charge due to distributed ions within the Nd_{1-x}-Sr_xCoO_{3-y} catalysts. The mobile electrons are associated with these charge transfers, but the density of energy levels available at the band edge is so low that the conduction electrons are spread any may be consiered as a space charge. This space charge can affect the electrical properties of $Nd_{1-x}Sr_x$-CoO_{3-y} and the double layers change the density of current cariers. The electron concentration for the CO oxidation may be controlled by such double layers.

As a result of adsorption of O_2 on the $Nd_{1-x}Sr_xCoO_{3-y}$ surface, the density of electrons at the surface of catalyst will decrease due to the formation of double layers, showing decreases in electrical conductivity with O_2. If O_2 is adsorbed on an oxygen vacancy defect, the electrical conductivity should decrease by the following equilibrium

$$O_2(g)+2e^- \xrightleftharpoons{k_1} 2O^- \text{ (ads)} \qquad (1)$$
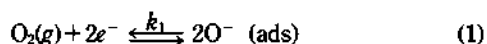
where e^- is a conduction electron which is produced by Sr substitution. The data in Table 3 indicate that equilibrium (1) moves to the right and that O_2 adsorbs on an oxygen vacancy defect, showing a possible site involved in adsorption of oxygen. The data in Table 3 also indicate that the conduction electron concentration increases with increasing CO adsorption. Considering that a lattice oxygen is a possible site involved in the CO adsorption, the electrical conductivity should increase according to the following equilibrium

$$CO(g)+O^{2-} \text{ (latt)} \xrightleftharpoons{k_2} CO_2(ads)+e^- \qquad (2)$$
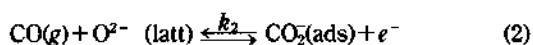
where the increases in P_{CO} move the equilibrium to the right and the electron concentration increases.

The kinetic data for CO oxidation on $Nd_{1-x}Sr_xCoO_{3-y}$ catalysts are found to obey closely the expression $-dp/dt=$ $kP^{1.5}_{CO+O_2}$ with respect to the total pressure in the reaction temperatures from 150 to 300℃ ; the total order was confirmed by the linearity shown in Figure 7. The rate constants listed in Table 1 are found to be compatible with the Arrhe-
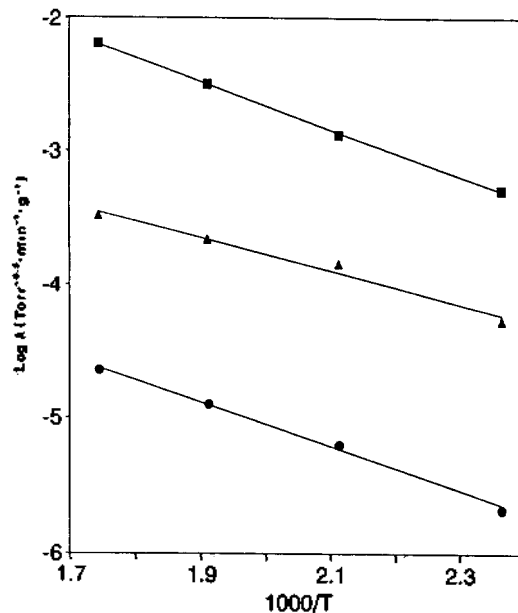

Figure 8. Arrhenius plot for the rates of CO oxidation on $Nd_{0.75}$-$Sr_{0.25}CoO_{2.992}$ (—●—), $Nd_{0.5}Sr_{0.5}CoO_{2.941}$ (—▲—) and $Nd_{0.25}Sr_{0.75}CoO_{2.897}$ (—■—) catalysts.

Table 2. Comparative Rates (r) of CO Oxidation as a Function of P_{CO} and P_{O_2} on $Nd_{1-x}Sr_xCoO_{3-y}$ Catalysts

| x	T (℃)	P_{CO}	P_{O_2}	r (Torr·min^{-1}·g^{-1})
0.25	150	120	60	1.99×10^{-3}
	150	119	30	1.40×10^{-3}
	150	60	29	0.69×10^{-3}
	300	120	60	2.08×10^{-2}
	300	120	29	1.45×10^{-2}
	300	59	30	0.73×10^{-2}
0.50	150	120	59	8.65×10^{-2}
	150	118	29	5.97×10^{-2}
	150	60	30	3.09×10^{-2}
	300	120	60	2.99×10^{-1}
	300	119	30	2.10×10^{-1}
	300	60	29	1.04×10^{-1}
0.75	150	119	60	4.66×10^{-1}
	150	120	30	3.29×10^{-1}
	150	59	30	1.62×10^{-1}
	300	120	59	5.82×10^{-0}
	300	118	30	4.08×10^{-0}
	300	59	29	2.00×10^{-0}

nius equation. Figure 8 shows the logarithm of the rate constant plotted against the reciprocal of the absolute temperature. The slopes of lines give 0.35, 0.25, and 0.33 eV, respectively. Table 2 shows the comparative rates obtained from the variation of P_{CO} and P_{O_2} on the three different $Nd_{1-x}Sr_x$-CoO_{3-y} catalysts within the same reaction temperature range. The exponents of the P_{CO} and P_{O_2} dependences are evaluated from the data in Table 2. The partial orders are found to

Kinetics, Mechanism, CO Oxidation, Nd$_{1-x}$Sr$_x$CoO$_{3-y}$

Bull. Korean Chem. Soc. **1994**, Vol. 15, No. 8 621

Table 3. Electrical Conductivities of Nd$_{0.5}$Sr$_{0.5}$CoO$_{2.941}$ under Various Partial Pressures of Carbon Monoxide and Oxygen at 300 ℃

Reactions	Partial pressures	Electrical conductivity $(\Omega \cdot cm)^{-1}$
Carbon Monoxide	28	1.75×10^2
	57	5.50×10^2
	90	1.52×10^3
	121	4.27×10^3
Oxygen	15	1.74×10^1
	30	5.51×10^0
	45	1.74×10^0
	60	6.15×10^{-1}

be first for CO and half for O$_2$. The half order with respect to O$_2$ implies that O$_2$ may adsorb on an oxygen vacancy and dissociate into two species, satisfying the equilibrium (1).

The kinetic data shown in Table 2 indicate that the elementary reaction (3) may be involved in the CO oxidation, since the reaction rates are increased with P_{CO} and P_{O_2}.

$$CO_2^-(ads) + O^-(ads) \xrightarrow{k} CO_2(g) + O^{2-}(latt) \quad (3)$$
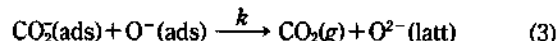
In order to test the inhibition effect of CO$_2$ and to know that the elementary reaction (3) is reversible or not, the CO$_2$ from the gas mixture was not frozen out by liquid nitrogen. The kinetic data obtained on Nd$_{1-x}$Sr$_x$CoO$_{3-y}$ catalysts without liquid nitrogen trap show 1.2 order with respect to the total pressure; the partial orders are found to be 0.7 for CO and 0.5 for O$_2$, indicating that CO$_2$ should be adsorbed on the catalyst surface. Therefore, the CO$_2$ inhibits the oxidation of CO and the reaction (3) should be represented as following equilibrium:

$$CO_2^-(ads) + O^-(ads) \rightleftharpoons CO_2(g) + O^{2-}(latt) \quad (4)$$
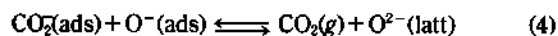
From equilibrium (1), $(O^-\ (ads)) = k_1^{1/2}(O_2)^{1/2}(e^-)$, from equilibrium (2), $(CO_2^-(ads)) = k_2(O^{2-}(latt))\ (CO)/(e^-)$, and from the elementary reaction (3), the rate of production of CO$_2$ can be represented as $d(CO_2)/dt = k(CO_2^-(ads))\ (O^-(ads))$. This rate equation can be rewritten with substitutions of $(CO_2^-(ads))$ and $(O^-(ads))$ as $d(CO_2)/dt = k\ k_1^{1/2}k_2(CO)(O_2)^{1/2}$, taking $(O^{2-}(latt))$ to be constant. This rate equation is consistent with experimental rate law and is as follows.

$$d(CO_2)/dt \cong k'(CO)(O_2)^{1/2} \quad (5)$$

Under the CO$_2$ inhibition, however, the rate law should be represented as $d(CO_2)/dt = k(\theta_{CO}/\theta_{CO_2})\ (\theta_{O_2})$ where θ_{CO}, θ_{CO_2}, and θ_{O_2} are surface coverages of CO, CO$_2$ and O$_2$, respectively. If the Langmuir's ideal adsorption is introduced into equilibria (1), (2) and (4), the rate law by the CO$_2$ inhibition should become as $d(CO_2)/dt = k((bP_{CO}/1+bP_{CO})/(bP_{CO_2}/1+bP_{CO_2}))\ (b^{1/2} P_{O_2}^{1/2}/1+b^{1/2}P_{O_2}^{1/2})$ where b is adsorption coefficient. The (V_o) may be very low, namely $\theta_{O_2} < 1$ and assuming that the equilibrium (1) is a rate controlling step and CO and CO$_2$ are chemisorbed on the same site of lattice oxygen, we can get

$$d(CO_2)/dt = ((k\ b_{CO} \cdot b_{O_2}^{1/2})/(b_{CO_2}))\ ((P_{CO}/P_{CO_2})^{\alpha}\ P_{O_2}^{1/2})$$

$$\cong k'(P_{CO}/P_{CO_2})^{\alpha}\ P_{O_2}^{1/2} \quad (6)$$

The rate of CO oxidation over Nd$_{1-x}$Sr$_x$CoO$_{3-y}$ catalysts shows 1.2-order kinetics; 0.7-order with respect to CO and 0.5-order to O$_2$. The kinetic data agree well with the rate law (6) with $\alpha = 0.7$ without a CO$_2$ trap. When a CO$_2$ trap is used, the oxidation of CO over all catalysts shows 1.5-order in total pressure; first-order with respect to CO and 0.5-order to O$_2$. The kinetic data agree will with eq. (6) when α becomes 1.

We can conclude on the basis of our experimental results that the formation of oxygen vacancy defect due to Sr substitution for Nd in NdCoO$_3$ solid phase is the important factor for the oxidation of CO on Nd$_{1-x}$Sr$_x$CoO$_{3-y}$ catalysts and in spite of the space charge on the catalyst surface, the catalytic activity would be related to its electrical properties and might be enhanced by Sr doping, showing that electron transfer during depletive adsorption of reactants on catalyst surface could not occur indefinitely.

References

1. Derouane, E. G. *Indi. Chim. Belg.* **1971**, *36*, 359.
2. Voorhoeve, R. J. H.; Johson, Jr. D. W.; Remeika, J. P.; Gallagher, P. K. *Science* **1977**, *195*, 827.
3. Kiss, J. T.; Gonzalez, R. D. *J. Phys. Chem.* **1984**, *88*, 898.
4. Gushee, B. E.; Katz, L.; Ward, R. *J. Am. Chem. Soc.* **1957**, *79*, 5601.
5. Laitenen, H. A.; Burdett, L. W. *Anal. Chem.* **1951**, *23*, 1268.
6. Choi, K. M.; Kim, K. H.; Choi, J. S. *J. Phys. Chem. Solids* **1988**, *49*, 1027.
7. Kim, K. H.; Yim, D. Y.; Choi, K. M.; Choi, J. S.; Sauer, Robert G. *J. Phys. Chem. Solids* **1989**, *50*, 1027.
8. Huong, P. V.; Oh-Kim, E.; Kim, K. H.; Kim, D.; Choi, J. S. *J. Less-Common Metal.* **1989**, *151*, 133.
9. Kim, D.; Choi, K. M.; Kim, K. H.; Choi, J. S. *J. Phys. Chem. Solids* **1989**, *50*, 821.
10. Kim, K. H.; Park, S. H.; Choi, J. S.; Hyung, K. W. *J. Phys. Chem. Solids* **1988**, *49*, 1019.
11. Won, H. J.; Park, S. H.; Kim, K. H.; Choi, J. S. *J. Phys. Chem. Solids* **1987**, *48*, 383.
12. Kim, Y. Y.; Kim, K. H.; Choi, J. S. *J. Phys. Chem. Solids* **1989**, *50*, 903.
13. Choi, J. S.; Lee, H. Y.; Kim, K. H. *J. Phys. Chem.* **1973**, *77*, 2430.
14. Choi, J. S.; Kang, Y. H.; Kim, K. H. *J. Phys. Chem.* **1977**, *81*, 2208.
15. Kim, K. H.; Han, H. S.; Choi, J. S. *J. Phys. Chem.* **1979**, *83*, 1286.
16. Kim, K. H.; Choi, J. S. *J. Phys. Chem.* **1981**, *85*, 2447.
17. Kim, K. H.; Kim, D.; Choi, J. S. *J. Catalysis* **1984**, *88*, 283.
18. Kim, K. H.; Lee, S. H.; Heo, G.; Choi, J. S. *J. Appl. Polym. Sci.* **1987**, *14*, 2537.
19. Kim, K. H.; Lee, S. H.; Heo, G.; Choi, J. S. *J. Phys. Chem. Solids* **1987**, *48*, 895.

20. Kim, K. H.; Jun, J. H.; Lee, S. H.; Choi, J. S. *J. Phys. Chem. Solids* **1989**, *50*, 785.
21. Choi, K. M.; Kim, K. H.; Choi, J. S. *J. Phys. Chem. Solids* **1989**, *50*, 283.
22. Choi, K. M.; Kim, K. H.; Choi, J. S. *J. Phys. Chem.* **1989**, *93*, 4659.
23. Choi, K. M.; Lee, E. J.; Park, J. W.; Kim, K. H. *J. Appl. Polym. Sci.* **1991**, *42*, 2129.
24. Cho, S. K.; Kim, D.; Choi, J. S.; Kim, K. H. *J. Phys. Chem. Solids* **1989**, *51*, 113.
25. Park, J. S.; Choi, K. M.; Kim, K. H.; Choi, J. S. *J. Phys. Chem. Solids* **1989**, *50*, 903.

26. Kim, K. H.; Yun, S. H.; Choi, J. S. *J. Phys. Chem. Solids* **1989**, *50*, 291.
27. Cho, E. K.; Chung, W. Y.; Choi, K. M.; Kim, K. H. *J. Am. Ceram. Soc.* **1990**, *73*, 3470.
28. Cho, S. K.; Kim, D.; Choi, J. S.; Kim, K. H. *J. Phys. Chem. Solids* **1989**, *51*, 113.
29. Kim, K. H.; Huong, P. V.; Oh-Kim, E.; Lalhaye, M.; Cho, S. K.; Kwak, B. C. *J. Less-Comm. Met.* **1990**, *164*, 1201.
30. Shaplygin, I. S.; Lazarev, V. B.; Russ, *J. Inorg. Chem.* **1985**, *30*, 1828.
31. Nakamura, T.; Misono, M.; Yoneda, Y. *J. Catal.* **1983**, *83*, 151.

Direct Solid Sample Analysis in the Moderate Power He Mip with the Spark Generation

S. R. Koirtyohann* and Yong-Nam Pak[†]

Department of Chemistry, Univeristy of Missouri, Columbia, MO 65201, U.S.A.
†*Department of Chemistry Education, Korea National University of Eduction, Cheong-Won, 363-791, Korea*
Received March 11, 1994

Conducting solid samples are successfully analyzed with the spark ablation combined to the moderate power (500 W) Helium Microwave Induced Plasma (He MIP). The relative standard deviations are in the range of 3-10% and the detection limits are around 50 μg g⁻¹. These values are higher than those of Ar MIP or Ar Inductively Coupled Plasma. Spark ablated particles are examined to investigate the analytical characteristics of the system.

Introduction

It is more advantageous analyzing a solid sample directly rather than dissolving it because of the time to dissolve and the risk of contamination from the chemicals used in the dissolution step. Also, the direct solid sample analysis should be inherently more sensitive when it is considered that only 1-2% of the total solution is delivered into the atomizer and the rest to a waste bottle. Thus, Arc/spark discharges have been used for the ICP[1-6] (Inductively Coupled Plasma) for conducting solid sample analysis.

Recent developments in the moderate power (up to 500 W) Helium and Argon Microwave Induced Plasmas (MIPs) have allowed them to be utilized in many spectroscopic areas[7-14] including MIP/Mass Spectrometry[12-14]. Their applications are well described in the review[15]. The Ar MIP has been used for metals while the He MIP has exclusively been used for non-metals such as halogens due to its high ionization potential available. The Ar plasma which has a desirable annular shape showed good analytical performances. The moderate power Ar MIP[10,11] gave good sensitivities and large dynamic ranges for metal ions even in aqueous samples of complex matrix.

On the other hand, the He MIP has been used mostly for the gaseous samples because of its low kinetic temperature[16]. Even the moderate power He MIP has shown insufficient vaporization of the samples and consequently, more

interferences and worse detection limits[8] than the Ar MIP. One reason is that a He plasma forms a cylindrical shape instead of a toroidal one. Thus, samples do not penetrate the hottest core of the plasma and show large interferences. In addition to that, the temperature and electron number density ($T_{rot} = 2,500$ K and 2.1×10^{14}/cm³) indicate[17] that the moderate power He MIP is not sufficiently "hot" in handling aqueous samples. However, the very high ionization temperature[17] of the He MIP provides its unusually high excitation capability.

In order to employ this efficient excitation character of a He plasma exclusively, "dried" particles are generated by the spark and introduced to the system. Since early works on the low power (100 W) He MIP with gaseous samples have been successful, it is expected that the "dried" particles introduced to the moderate power MIP should give good analytical results. Increasing power to a moderate level (up to 500 W) also should be a factor beneficial to the solid sample analysis. One of the purpose of this research is to examine the usefulness of the moderate power He MIP upon the introduction of "dried" particles. Analytical characteristics of the moderate power Spark/He MIP system will be compared with those of the Spark/Ar MIP system[18].

Experiment

Instrumentation